# Ion energy distribution and optical measurements in high-density, inductively coupled $C_4F_6$ discharges

Eric C. Benck,[a] Amanda Goyette, and Yicheng Wang
*National Institute of Standards and Technology, Gaithersburg, Maryland 20899-8421*

(Received 14 January 2003; accepted 1 May 2003)

Hexafluoro-1,3 butadiene ($C_4F_6$) is a potential etching gas with a very low global warming potential for the manufacturing of semiconductors, unlike commonly used fluorocarbon gases such as $CF_4$ and $c-C_4F_8$. We report ion energy distributions, relative ion intensities and absolute total ion current densities measured at the edge of an inductively coupled gaseous electronics conference radio-frequency reference cell for discharges generated in pure $C_4F_6$ and $C_4F_6$:Ar mixtures. In addition, the ratio of radical densities relative to CF measured using submillimeter absorption spectroscopy and optical emission spectroscopy measurements are presented. These measurements of the $C_4F_6$ plasmas were made for several different gas pressures (0.67, 1.33, and 2.66 Pa) and gas mixture ratios (25%, 50%, 75%, and 100% $C_4F_6$ volume fractions). © *2003 American Institute of Physics.* [DOI: 10.1063/1.1586978]

## I. INTRODUCTION

Low pressure radio frequency (rf) fluorocarbon discharges are commonly used in the manufacturing of microelectronics. Typically, saturated fluorocarbon gases such as $CF_4$ or $c-C_4F_8$ have been used, particularly with the etching of silicon and silicon dioxide. Unfortunately, there has been a growing concern over the ecological impact of these manufacturing processes. The 100 yr integrated global warming potential ($GWP_{100}$) relative to $CO_2$ for many of the commonly used fluorocarbon gases ($CF_4$ 5700, $c-C_4F_8$ 11299, and $CHF_3$ 14800) [1] are quite large and the concentration of these gases in the atmosphere has been consistently growing in recent years. Consequently, there has been an effort to identify alternative gas chemistries that are more environmentally benign. This not only includes reducing the environmental hazard of the initial feed gases used, but also reducing the total global warming impact of the etching process effluents.

One potential alternative etching gas is 1,3 hexafluorobutadiene ($C_4F_6$). This unsaturated fluorocarbon isomer of $C_4F_6$ has a chemical structure consisting of a zigzag chain of four carbon atoms. The central two carbon atoms have a single interconnecting atomic bond between them while double bonds attach the outer carbon atoms ($CF_2=CF-CF=CF_2$). The global warming potential of this gas is so low ($GWP_{100}=0.027$) [2] that it is typically ignored in global warming impact calculations. An initial study by Chatterjee *et al.* demonstrated an 80% decrease in global warming plasma emissions from a $C_4F_6$ based etching process when compared to a standard $C_3F_8$ etching process.[3]

This article will report on the ion and neutral densities within a high-density, inductively coupled plasma (ICP) source operating with pure $C_4F_6$ and $C_4F_6$:Ar mixtures for several different pressures and gas mixture ratios.

[a]Author to whom correspondence should be addressed.

## II. EXPERIMENTAL APPARATUS

### A. Plasma reactor

The plasmas examined in this paper were created in a modified inductively coupled gaseous electronics conference (GEC) reference cell.[4,5] The plasma source, along with the ion-energy analyzer and mass spectrometer, are shown schematically in Fig. 1. The plasma is created with a flat five turn spiral coil separated from the plasma by a 9.5 mm thick fused silica vacuum interface. An additional fused silica confinement ring is attached to the coil assembly to improve the plasma stability and increase the operating range. The feed gas enters the cell through one of the 2.75 in. side flanges and is pumped out through the 6 in. port attached to a turbomolecular pump. The gas pressure is maintained by a variable gate valve between the pump and the GEC cell. The gas flow was maintained by mass flow controllers at 3.73 or 7.45 $\mu$mol/s (5 or 10 sccm). When gas mixtures are used, the percentages reported in this article are based on the volume fraction of the gases.

The discharge was generated by applying a 13.56 MHz voltage to the coil through a matching network. The rf power values presented in this article are the net power to the matching network driving the coil. The actual rf power dissipated in the plasma has been determined to be approximately 80% of the power listed.[5] The lower electrode was water cooled (20 °C) and grounded to the vacuum chamber. A 137.9 mm diam stainless steel plate with a bare 100 mm diam silicon wafer on top was centered on the lower electrode. A gap of approximately 2.54 cm exists between the lower electrode and the quartz confinement ring.

### B. Mass spectrometer and Faraday cup

The energy analyzer/mass spectrometer was mounted on a side port as shown in Fig. 1 with the inlet orifice grounded. In order to sample the ions closer to the center of the discharge, an extension has been added to the end of the mass

 

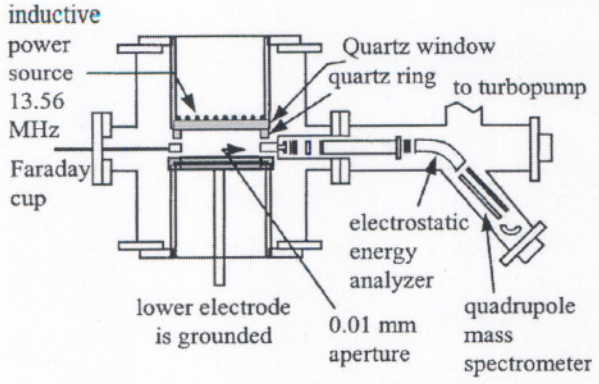


FIG. 1. Schematic diagram of the GEC rf reference cell and the side mounted mass selective ion energy analyzer.

spectrometer.[6] The ions are therefore sampled through a 10 $\mu$m diam hole located 9.5 mm above the steel plate and 46 mm from the radial center (11 mm inside the inner diameter of the confinement ring). The resolution of the energy analyzer [full width at half maximum (FWHM)] was 1 eV, and the uncertainty in its energy scale is estimated to be $\pm 1$ eV. Ion intensities were adjusted to account for previously measured variations in ion transmission as a function of ion mass.[7] After such adjustments, the ion transmission is estimated to be uniform to 20% over the range of ion masses and ion energies studied here.

To calibrate the ion fluxes measured by the mass spectrometer, a Faraday cup was mounted on a 2.75 in. side port. The 1.59 mm diam aperture at the inlet of the Faraday cup was positioned at the same radius and height as the mass spectrometer orifice. The dc current measured when the cup was dc biased at $-20$ V was divided by the area of the aperture to obtain the total ion current density. This value was then used to normalize the relative ion fluxes measured by the mass spectrometer.

### C. Submillimeter absorption diagnostic

Submillimeter absorption spectroscopy is a new diagnostic being developed at NIST for monitoring the neutral radicals in semiconductor processing plasmas.[8] Submillimeter radiation couples to the rotational spectra of molecules, as opposed to the vibrational modes probed by infrared radiation and electronic states by ultraviolet (UV) radiation. Almost all noncentrosymmetric molecules that have an intrinsic electric dipole moment have strong absorption spectra in this frequency region. The measurements presented in this paper are some of the earliest measurements using this technique on etching type plasmas and the diagnostic is still undergoing further development.

The submillimeter radiation source for these measurements was a backward wave oscillator (BWO). This continuous wave electron tube device acts as a voltage controlled frequency source. It can be referenced to an atomic clock or crystal oscillator for exceptional frequency metrology. The radiation has a linewidth on the order of 10 kHz. The particular BWO used with these measurements had a spectral range from approximately 450 GHz to 650 GHz. With this single source, it is possible to measure the absorption spectra

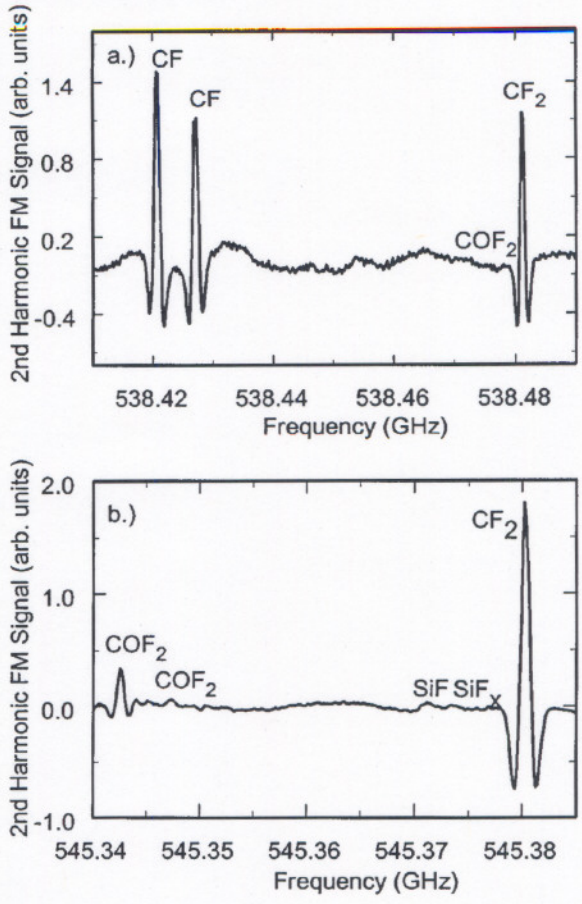


FIG. 2. Submillimeter absorption spectra signals for pure $C_4F_6$ plasma at 1.33 Pa (10 mTorr), 3.37 $\mu$mol/s (5 sccm), and 200 W 13.57 MHz rf power.

from almost all the molecules of interest. The submillimeter radiation transmitted through the plasma is detected with a liquid helium cooled Nd bolometer.

Second harmonic frequency modulation (FM) was used to detect the molecular absorption signals. Two typical absorption spectra are shown in Fig. 2. Use of the second harmonic FM technique improves the resulting signal to noise ratio, but also eliminates the dc background transmission necessary for absolute density calculations. The experimental data was fitted with a model function based on the second derivative of a Gaussian line shape with a third order polynomial background. This second derivative approximation works well as long as the FM depth is small compared to the absorption linewidth. The approximation significantly reduces the computational time necessary to analyze the signals compared to a more accurate modeling of the FM signal from a Voigt line shape.

The optical transitions used for measuring the radical densities are shown in Fig. 2. The transitions were 538.420 6921 and 538.427 1924 GHz for CF, 538.481 47 and 545.380 3254 GHz for $CF_2$, 545.342 6713 GHz for $COF_2$, and 545.3706 GHz for SiF. Except for SiF, line strengths for these molecular transitions have been calculated or found in the literature[9,10] for a temperature of 300 K. Measurements of the Doppler width with the BWO in the present experimental configuration has consistently found temperatures

close to or only slightly above room temperature. By taking ratios of the transitions, the uncertainty in the BWO intensity and optical path length can be eliminated. The error bars of all the submillimeter based measurements are not calculated from the standard deviation of multiple measurements, but from the maximum residual between the curve fit and the original data. While this does not give a true measure of the uncertainty in the data, it does give a rough estimate of the how well the model fitted the data and the reliability of the measurements.

Other plasma diagnostics, such as laser induced fluorescence, have found rotational gas temperatures ($>500$ K) significantly higher than room temperature in similar ICP sources.[11–13] This implies that the submillimeter absorption measurements are preferentially sensitive to cooler gas in the region surrounding the plasma. This is in part due to the geometry of the vacuum chamber used in these measurements. The path length through the surrounding gas is two times as long as that through the actual plasma. This is much different than what would be found in most commercial etching reactors. In addition, the density of the plasma gases is inversely proportional to the temperature and the signal amplitude is even further reduced due to the increased Doppler linewidths. As a result, the gas in the plasma makes only a small contribution to the total line-integrated submillimeter absorption signal.

### D. Optical emission

Optical emission from the plasma was collected with a quartz optical fiber which viewed the plasma through a quartz window on a 2.75 in. flange. No collimating optics were used so that spatially averaged light from the entire plasma volume was collected. The spectra were then measured with a small optical multichannel analyzer. The data were not corrected for wavelength dependent transmission and detection efficiencies. The spectrometer response function had a FWHM linewidth of 1.5 nm.

## III. RESULTS AND DISCUSSION

### A. Pure $C_4F_6$

Figure 3a shows the mass spectrum of the ions produced in a pure $C_4F_6$ plasma at 1.33 Pa (10 mTorr) and 200 W. $CF^+$ is the dominant ion, but there are significant contributions from $CF_2^+$ and from the $SiF_x^+/COF_x^+$ ions. Although electron-impact ionization cross sections have not been measured for this isomer of $C_4F_6$, comparison with ion yields produced by 70 eV electron bombardment [Fig. 3(b)] shows a marked dissimilarity in the relative yields of aliphatic ions such as $C_3F_3^+$ and $C_4F_6^+$ (not shown), which are almost completely absent in the plasma. The relatively low molecular weight of the plasma ions suggests a high degree of dissociation of the parent gas, and the significant proportion of ions which contain either Si or O indicates a considerable contribution from surface reactions to the overall ion chemistry. This is very different from inductively coupled $CF_4$ discharges measured in the same chamber which showed ion mass distributions that could be attributed mainly to direct electron impact of the feed gas,[14] but is similar to other fluorocarbon etching gases such as $C_2F_6$ and $c-C_4F_8$.[15] It is worth noting that electron attachment to $C_4F_6$ occurs at low energies with appreciable rates,[16,17] and presents a likely decomposition channel that is of much lesser importance in $CF_4$.

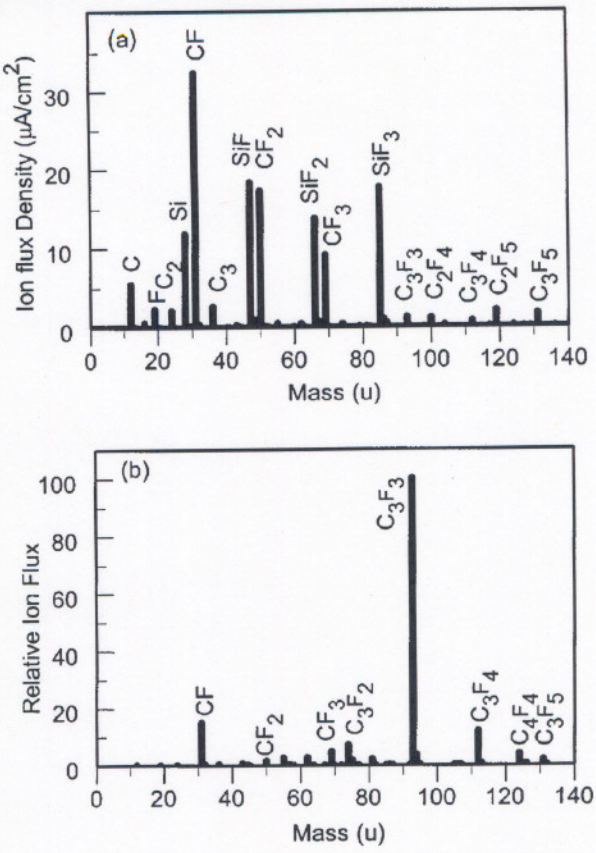


FIG. 3. (a) Mass spectrum of ions from the GEC cell from a 200 W, 133 Pa $C_4F_6$ discharge; (b) expected ion flux due to 70 eV electrons dissociating $C_4F_6$.

The total ion flux of these $C_4F_6$ discharges are approximately 1 order of magnitude lower than what we have previously measured for $C_2F_6$ and $c-C_4F_8$ (2 – to 5 mA/cm$^2$).[15] These measurements were made from the center of the lower electrode without a fused silica confinement ring present. The inductively coupled GEC reference source has a relatively strong radial variation in the plasma density as measured previously with Langmuir probes and optical emission tommography.[18,19] Switching the measurement location from the plasma center to the edge without the confinement ring drops the measured ion flux by a factor of 4. The fused silica confinement ring will also reduce the ion flux escaping to the edges of the plasma. In addition, $C_4F_6$ is a highly polymerizing plasma. This could result in the depostion of an insulating film on either the mass spectrometer or the Faraday cup introducing a systematic error. Consequentially, greater emphasis should be placed on the relative ion densities than on the quoted absolute values presented in this article.

The resolution of the mass spectrometer is not sufficient to distinguish between the Si and CO masses, so there re-

mains an uncertainty to the identity of the $SiF_x^+/COF_x^+$ ions. Etching of the fused silica window and confinement ring beneath the induction coil could be a source of both oxygen and silicon for the plasma. Because no rf bias is applied to the lower electrode, a relatively thick fluorocarbon layer is deposited on the silicon wafer which should limit the wafer as a source of silicon in the plasma.[20] Additional oxygen could come from the dissociation of water vapor in the plasma chamber, but if this were a significant source there should be more hydrogen containing molecular ions such as $HF^+$ within the plasma. Utilizing the isotopic ratios to distinguish between CO and Si containing molecular ions produced inconsistent results. The isotopic ratios measured with the mass spectrometer indicate that the lowest mass ions (28 u) are mostly $CO^+$ molecular ions, while the higher mass ions seem to be almost entirely $SiF_x^+$ molecular ions. Although the lower electrode is cooled, the current experimental setup does not ensure good thermal contact between the wafer and the electrode and consequently the wafer surface may become heated and affect the silicon etch rate. This could become a significant issue if the lower electrode is biased resulting in a significant ion flux to the silicon surface.

Representative ion energy distributions (IEDs) of the five most abundant ions are shown in Fig. 4(a). It is clear that the measured ion energy distributions are being significantly modified by the time varying sheath electric fields. Figure 4(b) shows several IEDs with the same plasma conditions which have been normalized to have the same maximum intensity. The IEDs show a definite mass dependant width between the double peaks. This is very different from other less electronegative gasses such as $CF_4$ in which the IEDs have a single peak.[14] Based on the sheath models of Sobolewski *et al.*,[6] the IED width should depend on both the ion mass and the time varying component of the voltage across the sheath.[21,22] Since the mass spectrometer orifice is grounded, the voltage across the sheath should represent the fluctuations of the plasma potential. According to Ref. 6 Eqs. (24) and (17), the width of the IEDs ($\Delta E$) is related to the ion mass ($m_i$) and the peak-to-peak voltage ($V_{pp}$) across the ground sheath at the mass spectrometer orifice by the function $\Delta E = eV_{pp}[1+Am_i]^{-1/2}$, where $A$ is considered constant. This function has been fitted to the measured IEDs for each plasma condition to determine $V_{pp}$. The IED width was measured between the maxima of the side peaks. Figure 4(c) shows how this model function fits with the experimentally measured IED widths.

Figure 5 shows the ion flux dependence on pressure. The overall ion flux shows a decrease with increasing pressure over the range from 0.67 to 2.66 Pa (5 – 20 mTorr). This is consistent with most of the fluorocarbon gases previously studied in this plasma source, except for $C_2F_6$.[14,15,23] The total flux was significantly lower than the other fluorocarbon gases measured in the same vacuum chamber and is probably due to sampling the flux from the side of the plasma instead of through the center of the grounded lower electrode. $CF^+$ remains the dominant ion over the entire pressure range, but there are strong contributions from the other molecular ions. At 0.67 Pa, $CF_2^+$ is the second most intense ion flux while at 2.66 Pa $SiF^+/COF^+$ and $SiF_3^+/COF_3^+$ become the second most abundant ions. $CF^+$ and $CF_2^+$ show a decrease in flux with increasing pressure, while $CF_3^+$ shows essentially no dependence. The $SiF_x^+$ ($x=1-3$) ions have a maximum flux at the intermediate pressure of 1.33 Pa. Atomic ion fluxes of $C^+$ and $Si^+/CO^+$ as well as $C_2^+$ decrease rapidly with increasing pressure. $C_3^+$, on the other hand, increases with increasing pressure. This increase in $C_3^+$ may be indicative of increasingly favorable conditions within the plasma for the formation of larger carbon clusters and particulates as the pressure is increased.

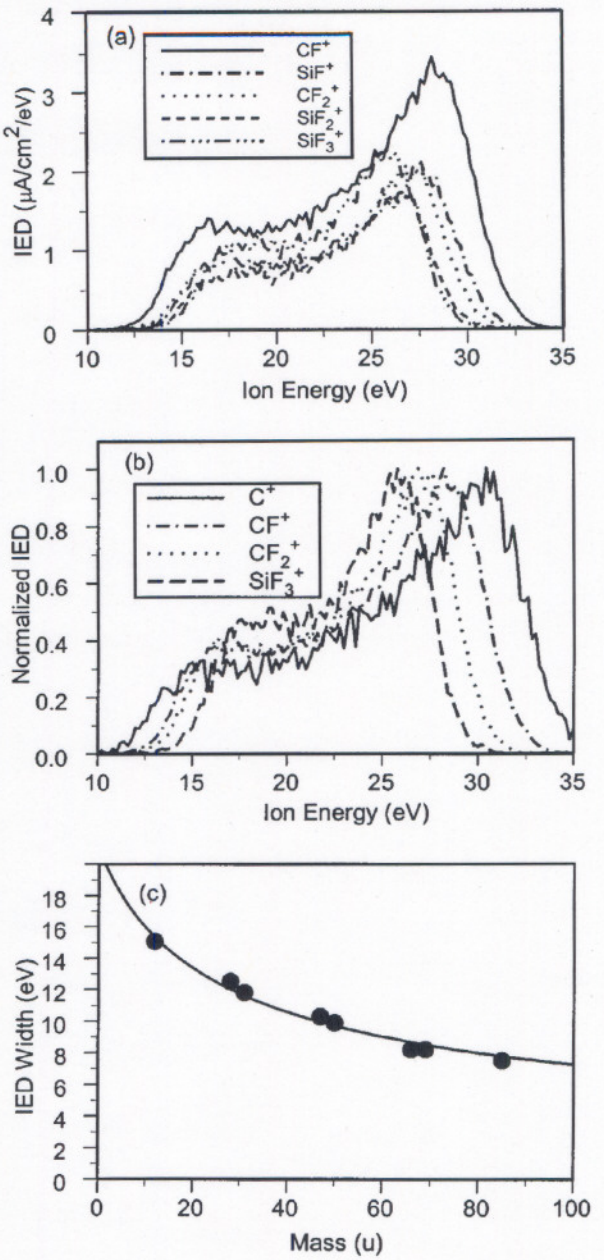


FIG. 4. (a) Ion energy distributions of the five dominant ions produced in a 200 W, 1.33 Pa $C_4F_6$ plasma. The absolute flux density of individual ion species was obtained by normalizing the total counts of the mass scan to the total current measured through the mass spectrometer orifice. (b) Normalized ion energy distributions for the same plasma conditions. (c) Model linewidth function fitted to the experimentally determined ion energy linewidths for the same plasma conditions.

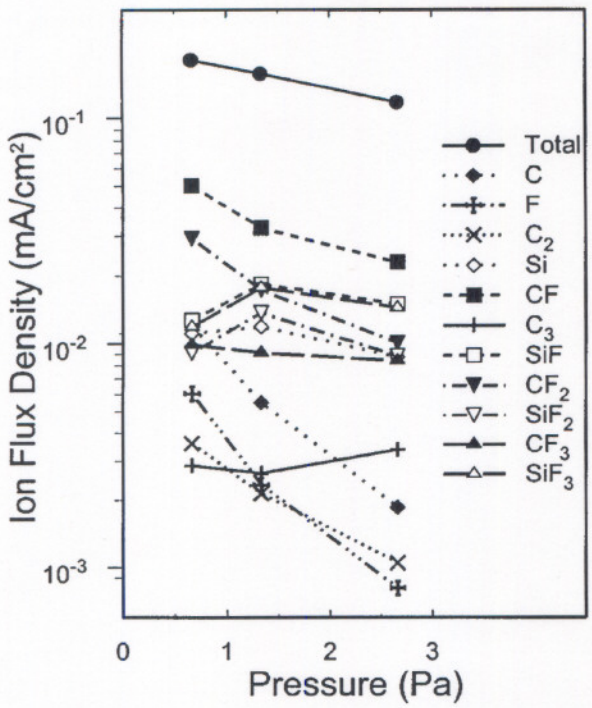


FIG. 5. Mass analyzed ion flux measured for a 200 W, $C_4F_6$ plasma as a function of pressure.

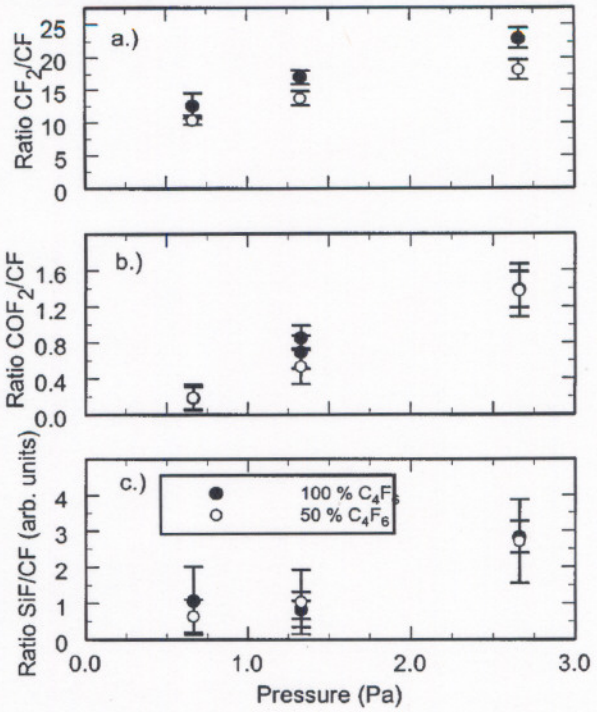


FIG. 7. Density ratios determined from the submillimeter absorption measurements of: (a) $CF_2/CF$, (b) $COF_2/CF$, and (c) SiF/CF for a 200 W, 1.33 Pa for a pure $C_4F_6$ and a 50% $C_4F_6$:50% Ar mixture. The SiF/CF ratio is not on an absolute scale. The error bars do not represent the true statistical uncertainty of the measurements, but were determined from the maximum residual between the model lineshape and the original data.

Figure 6 shows how the IED of $CF^+$ changes with pressure. The IEDs of all three pressures show the characteristic double peak distribution. The intermediate pressure, 1.33 Pa, has the greatest width. This differs from what we have observed in inductively coupled discharges generated in other fluorocarbon gases,[15] in which the IEDs typically broaden monotonically with increasing pressure.

The submillimeter absorption spectroscopy results differed from the ion mass spectroscopy. This is shown in Fig. 7. The $CF_2$ radical is significantly more abundant than CF and the ratio increases with increasing pressure. This is probably due to the enhanced sensitivity to the region outside of the plasma. The path length through the cooler region outside the plasma is approximately twice as long as the path through the hotter, less dense gas in the actual plasma. $CF_2$ molecules can also be produced by surface reactions as well as collisional dissociation. $CF_2$ produced at surfaces is probably diffusing from the outer walls towards the plasma where it is dissociated by the plasma. Consequentially, the $CF_2/CF$ ratio is probably smaller in the actual plasma. The density of $COF_2$ is comparable to that of CF, but the signal-to-noise ratio of the measurements is much poorer due to lower sensitivity for the $COF_2$ molecules. Accurate line strength data for SiF are not currently available, so the SiF/CF ratio could not be put on an absolute ratio scale. But both the $COF_2$ and SiF ratios show similar trends of increasing density relative to CF with increasing pressure. Since both $COF_2$ and SiF radicals are present in the plasma, this may indicate that analogous ion fluxes are mixtures of $COF_x^+$ and $SiF_x^+$.

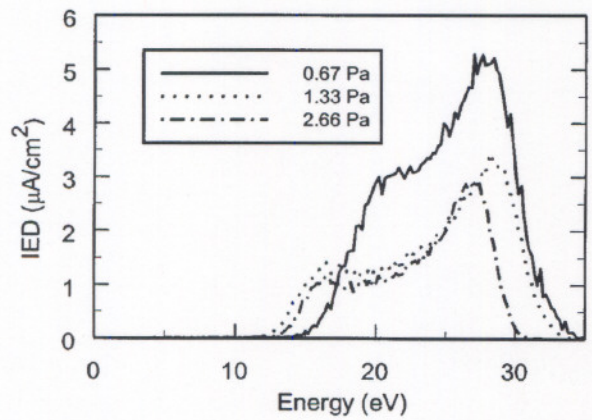


FIG. 6. Ion energy distributions for $CF^+$ ions sampled from a 200 W, $C_4F_6$ plasma as a function of pressure.

Figure 8 shows a typical optical emission spectroscopy measurements obtained from the plasma. The optical spectra are dominated by the molecular carbon Swan bands along with bands from SiF. There is an additional band peaking around 405 nm which is probably due to $C_3$. Small atomic transition lines can be observed from both fluorine in the red and silicon in the UV. Several very weak signals around 260 nm may also be due to $CF_2$. The F signal decreased with increasing pressure while the SiF and Si OES signals had maxima at the intermediate pressure of 1.33 Pa. The $C_3$ and $C_2$ bands increased with increasing pressure. The ratio of the $C_3/C_2$ signals also increases with increasing pressure. This

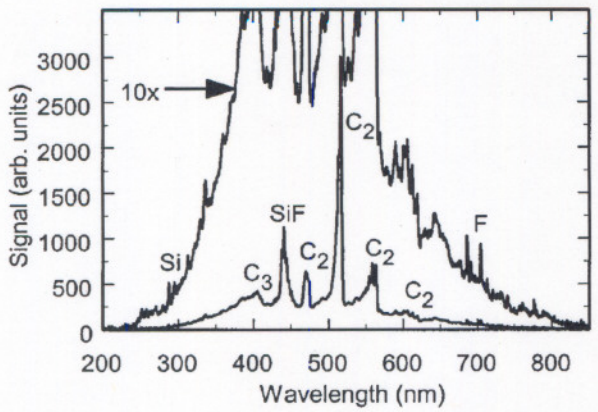


FIG. 8. Optical emission spectra from a 200 W, 1.33 Pa $C_4F_6$ discharge.

may indicate developing conditions favorable for the growth of carbon particulates.

### B. $C_4F_6$:Ar mixture

Figure 9 shows the total ion flux and flux of component ions for an inductively coupled plasma sustained in $C_4F_6$:Ar gas mixtures with a pressure of 1.33 Pa (10 mTorr) at 200 W. The total ion current demonstrates a slow decrease with increasing $C_4F_6$ input concentration. This is probably due to increasing power being necessary to dissociate the molecular components. In the mixtures, the dominant ion was always $Ar^+$, although the ion flux was dropping proportionally with decreasing percentage of Ar. $CF^+$ had the second highest flux followed by $CF_2^+$, $SiF^+/COF^+$, and $SIF_3^+/COF_3^+$ which

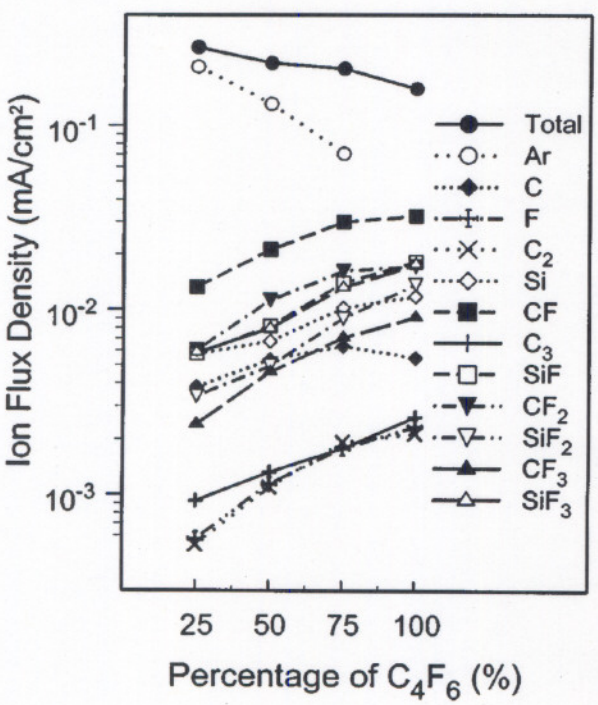


FIG. 9. Mass analyzed ion flux, as a function of $C_4F_6$:Ar mixtures for a 200 W and 1.33 Pa plasmas.

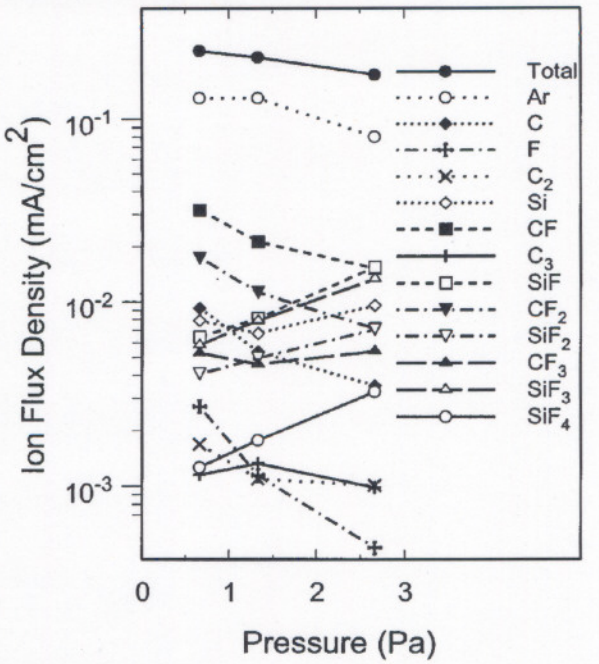


FIG. 10. Mass analyzed ion flux, as a function of pressure for a 50% $C_4F_6$:50% Ar mixtures for a 200 W and 1.33 Pa plasmas.

all had similar ion fluxes. Except for $Ar^+$ and $C^+$, all the ion fluxes increased with increasing percentage of $C_4F_6$. It is interesting to note that although the fluxes of both $CF^+$ and $CF_2^+$ increased almost proportionally with $C_4F_6$ addition from 25% $C_4F_6$ to 75% $C_4F_6$, the fluxes of both ions showed a similar leveling off as the mixture approached 100% $C_4F_6$, whereas the flux of $CF_3^+$ continued to increase in proportion to $C_4F_6$ addition.

Figure 10 shows the total ion flux and the flux of component ions for an inductively coupled plasma sustained in a 50% $C_4F_6$:50% Ar mixture at 200 W as a function of gas pressure. The magnitude of the total ion flux exhibits a slight downward trend over the pressure range from 0.67 to 2.66 Pa (5 – 20 mTorr), similar to that observed in other fluorocarbon:argon mixtures.[14,15,23] The dominant ion under all conditions is $Ar^+$, similar to the behavior of $CHF_3$. As with the case of pure $C_4F_6$, the total flux was significantly lower than the other fluorcarbon gases measured in the same vacuum chamber.

Of particular interest is the differing behavior of the $CF_x^+$ and $SiF_x^+/COF_x^+$ $(x=0-4)$ ions. As with the pure $C_4F_6$ discharges, there is a general shift in the ion composition from fluorocarbon ions to secondary ions which originate from etching byproducts as the pressure is increased, again underscoring the contributions of these processes to the overall ion chemistry. The fluxes of most of the fluorocarbon ions decrease with increasing pressure with the exception of $CF_3^+$, which showed a slight increase at the highest pressure. The $SiF_x^+$ molecular ions showed the exact opposite behavior, increasing ion flux with increasing pressure. The fluxes of atomic ions (except Ar) were very small and strongly decreased with increasing pressure.

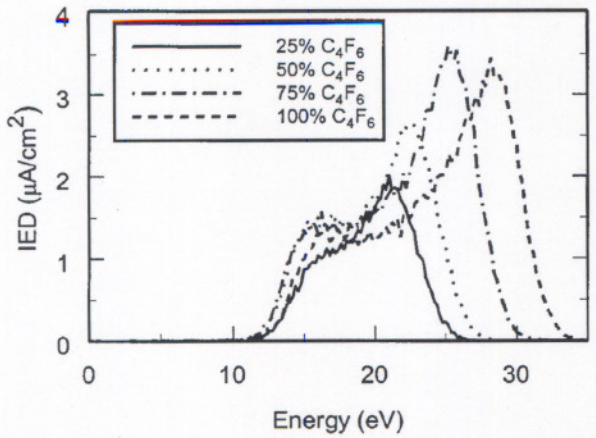


FIG. 11. Ion energy distributions for $CF^+$ ions sampled from a 200 W, 1.33 Pa plasmas for several $C_4F_6$:Ar gas mixtures.

Figure 11 shows representative IEDs of $CF^+$ for $C_4F_6$:Ar mixtures for various plasma conditions. The average energies of these IEDs are roughly 5 V lower than those for the pure $C_4F_6$ discharges shown in Fig. 6. In addition, the IEDs are narrower and at the lowest pressure (0.67 Pa) the dual peak IED is beginning to combine into a single peak as shown in Fig. 12. Figure 13 shows how the width of the plasma potential oscillations, determined from the curve fitting procedure described previously, changes with pressure and percentage of $C_4F_6$. Increasing the percentage of $C_4F_6$ in the plasma increases the peak to peak voltage oscillations. Increasing the flow rate seems to increase the amplitude of the oscillations slightly. The dependence on pressure was more complicated. The pure $C_4F_6$ plasma potential oscillations had a maximum at 1.33 Pa while the 50% $C_4F_6$ mixture continued to increase with pressure. These values are significantly larger than those measured directly using a wire loop probe in Ar and $CF_4$ discharges (on the order of $1-2$ V).[6,24] We have not directly measured the plasma oscillations in other more similar fluorocarbon discharges, but the IED widths of such feedgases as $C_2F_6$ and $c-C_4F_8$ are smaller than $C_4F_6$ but are at least comparable in magnitude.[6,15,24]

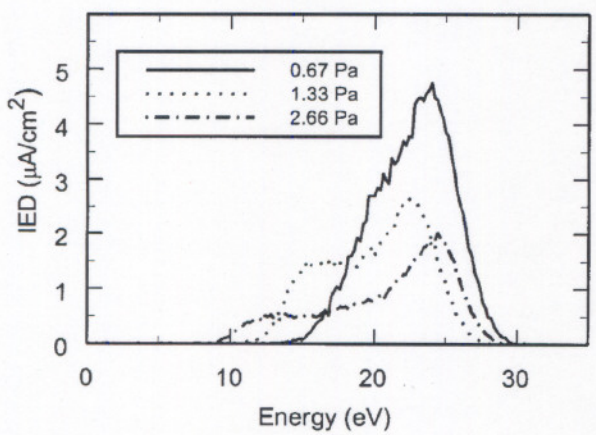


FIG. 12. Ion energy distributions for $CF^+$ ions sampled from a 200 W, 50% $C_4F_6$:50%Ar plasmas for several different pressures.

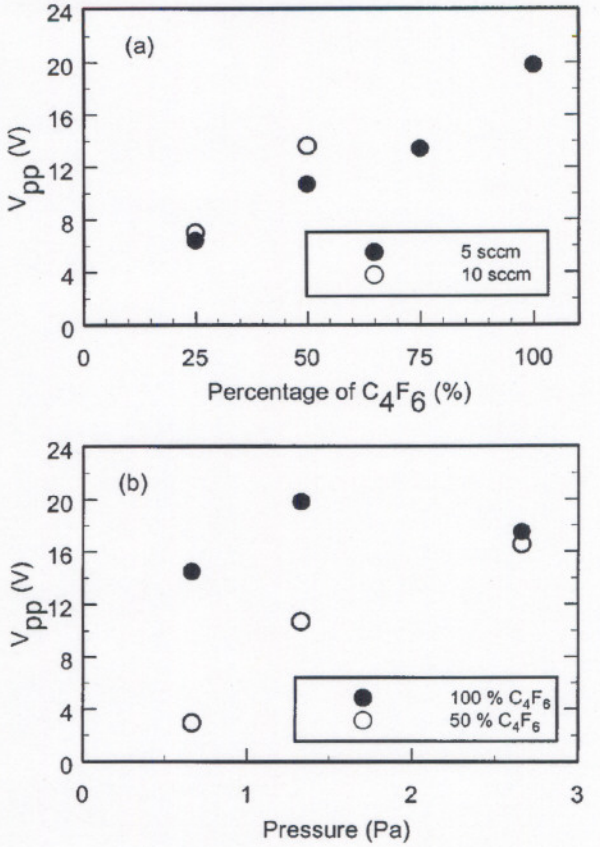


FIG. 13. Plasma potential oscillations determined from the effective width of the IEDs for several widths for (a) different flow rates as a function of the percentage of $C_4F_6$ in the gas mixture at a pressure of 1.33 Pa and (b) different gas mixtures as a function of pressure at a flow rate of 3.37 μmole/s (5 sccm).

There appears to be a large contribution of capacitve coupling to these discharges, probably related to the high electronegative nature of these plasmas.

The neutral radical ratios measured with the submillimeter absorption diagnostic are shown in Fig 14. The $CF_2/CF$ ratio increases from approximately 10 to 16 as the percentage of $C_4F_6$ changes from 25% to 100%. It is also clear that increasing the flow rate also increases the $CF_2/CF$ ratio in this relatively low flow rate range. The signal-to-noise ratios of the $COF_2$ and SiF signals are unfortunately too low to make any significant comments about how their ratios change with the varying $C_4F_6$ gas mixture.

The optical emission spectra of the $C_4F_6$:Ar mixtures is very similar to the pure $C_4F_6$ plasmas with the addition of strong Ar transitions in the red region of the spectra. With a 50% $C_4F_6$:50% Ar mixture, the OES signals have similar behavior with pressure as the pure $C_4F_6$ plasma with the exception of SiF band which continues to increase with increasing pressure. The Ar transitions have a maximum at the intermediate pressure of 1.33 Pa. One significant difference is the ratio of the $C_3/C_2$ signals, which decreases with increasing pressure. This may indicate that the addition of Ar to the plasma might help suppress the growth of carbon particulates.

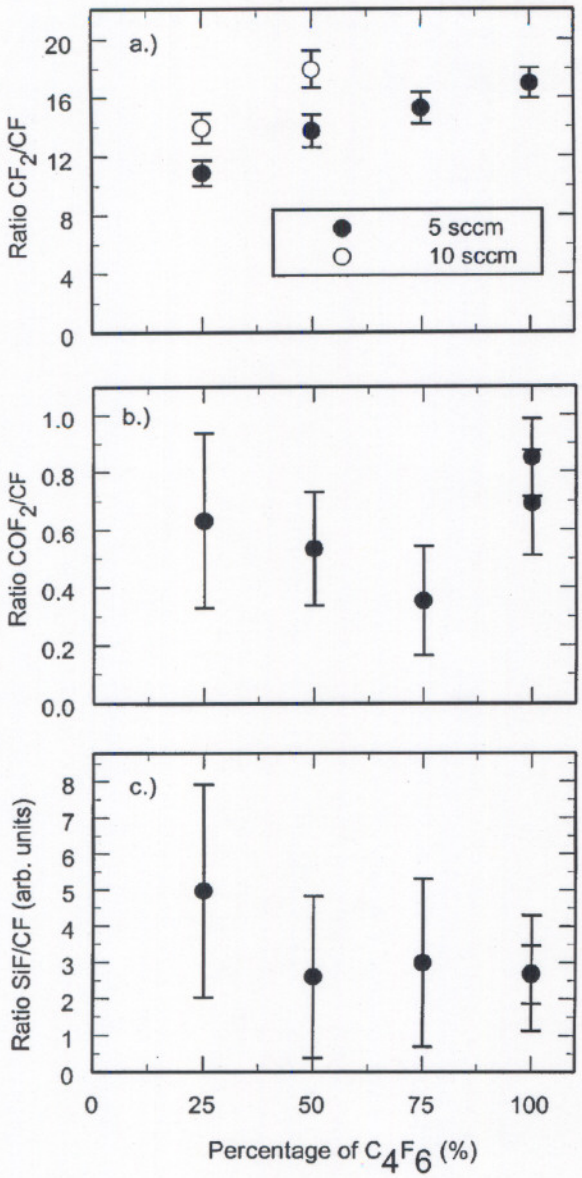


FIG. 14. Density ratios determined from the submillimeter absorption measurements of (a) $CF_2$/CF, (b) $COF_2$/CF, and (c) SiF/CF for a 200 W, 1.33 Pa for a 50% $C_4F_6$:50% Ar mixture at two different flow rates. The SiF/CF ratio is not on an absolute scale. The error bars do not represent the true statistical uncertainty of the measurements, but were determined from the maximum residual between the model line shape and the original data.

## IV. SUMMARY

The mass-analyzed ion flux densities have been measured for inductively coupled rf plasmas in pure $C_4F_6$ and in mixtures of $C_4F_6$ with Ar. The dominant ion in pure $C_4F_6$ was $CF^+$ and in the $C_4F_6$:Ar mixtures it was $Ar^+$ with $CF^+$ as the most abundant fluorocarbon ion. In all cases, there were strong ion fluxes due to etching byproducts ($SiF_x^+/COF_x^+$) even though there was no bias applied to the lower electrode. The etchant ions $CF_x^+$ tended to exhibit trends different from the etching byproducts $SiF_x^+/COF_x^+$ as plasma conditions were varied. The higher mass carbon molecular ions ($C_3^+$) increased relative to the lighter carbon ions ($C^+, C_2^+$) as gas pressure increased and may indicate the development of plasma conditions suitable for carbon particulate growth. Similar behavior was also seen in the optical emissions of $C_3$ and $C_2$.

The submillimeter absorption measurements found that $CF_2$ density was approximately ten times greater than CF. The etching byproduct $COF_2$ had a density comparable to CF. SiF/CF ratio could not be put on an absolute scale, but showed similar trends as $COF_2$/CF ratio as plasma conditions were varied.

The ion energy distributions functions were double peaked, showing that the ions crossing a ground sheath are significantly modified by the time varying electric fields. Analysis of the IED widths showed that the plasma potential oscillations increase with increasing $C_4F_6$ concentration. The plasma potential oscillations did not monotonically increase with increasing pressure in a pure $C_4F_6$ discharge, but did in a 50% $C_4F_6$:50% Ar mixture.

## ACKNOWLEDGMENT

The authors would like to acknowledge Ausimont USA for providing the $C_4F_6$ used in these experiments.

[1] Report No. 44, 1998.
[2] G. Acerboni, J. A. Beukes, N. R. Jensen, J. Hjorth, G. Myhre, C. J. Nielsen, and J. K. Sundet, Atmos. Environ. **35**, 4113 (2001).
[3] R. Chatterjee, S. Karecki, R. Reif, V. Vartanian, and T. Sparks, J. Electrochem. Soc. **149**, G276 (2002).
[4] P. J. Hargis, Jr., *et al.* Rev. Sci. Instrum. **65**, 140 (1994).
[5] P. A. Miller, G. A. Hebner, K. E. Greenberg, P. D. Pochan, and B. P. Aragon, J. Res. Natl. Inst. Stand. Technol. **100**, 427 (1995).
[6] M. A. Sobolewski, Y. Wang, and A. Goyette, J. Appl. Phys. **91**, 6303 (2002).
[7] Y. Wang and J. K. Olthoff, J. Appl. Phys. **85**, 6358 (1999).
[8] E. C. Benck, G. Y. Golubiatnikov, and G. T. Fraser, J. Vac. Soc. Technol. A (2002).
[9] H. M. Pickett, R. L. Poynter, E. A. Cohen, M. L. Delitsky, J. C. Pearson, and H. S. P. Muller, J. Quant. Spectrosc. Radiat. Transf. **60**, 883 (1998).
[10] H. S. P. Muller, S. Thorwirth, D. A. Roth, and G. Winnewisser, Astron. Astrophys. **370**, L49 (2001).
[11] H. Abada, P. Chabert, J. Booth, J. Robiche, and G. Cartry, J. Appl. Phys. **92**, 4223 (2002).
[12] G. A. Hebner, J. Appl. Phys. **80**, 2624 (1996).
[13] B. A. Cruden, M. V. V. S. Rao, S. P. Sharma, and M. Meyyappan, J. Appl. Phys. **91**, 8955 (2002).
[14] J. K. Olthoff and Y. Wang, J. Vac. Sci. Technol. A **17**, 1552 (1999).
[15] A. N. Goyette, Y. Wang, M. Misakian, and J. K. Olthoff, J. Vac. Sci. Technol. A **18**, 2785 (2000).
[16] I. Sauers, L. G. Christophorou, and J. G. Carter, J. Chem. Phys. **71**, 3016 (1979).
[17] A. A. Christodoulides, L. G. Christophorou, R. Y. Pai, and C. M. Tung, J. Chem. Phys. **70**, 1156 (1979).
[18] A. Schwabedissen, E. C. Benck, and J. R. Roberts, Phys. Rev. E **55**, 3450 (1997).
[19] E. C. Benck and K. Etemadi, in *Fiber Optic Based Optical Tomography Sensor for Monitoring Plasma Uniformity 2000, Gaithersburg MD,* Proceedings of the Conference on Characterization and Metrology for USLI Technology 2000, AIP Conf. Proc. No. 550 (AIP, Melville, NY, 2001), p. 268.
[20] X. Li, X. Hua, L. Ling, and G. S. Oehrlein, J. Vac. Sci. Technol. A **20**, 2052 (2002).
[21] P. A. Miller and M. E. Riley, J. Appl. Phys. **82**, 3689 (1997).
[22] C. Charles, A. W. Degeling, T. E. Sheridan, J. H. Harris, M. A. Lieberman, and R. W. Boswell, Phys. Plasmas **7**, 5232 (2000).
[23] Y. Wang, M. Misakian, A. N. Goyette, and J. K. Olthoff, J. Appl. Phys. **88**, 5612 (2000).
[24] M. A. Sobolewski, Phys. Rev. E **59**, 1059 (1999).